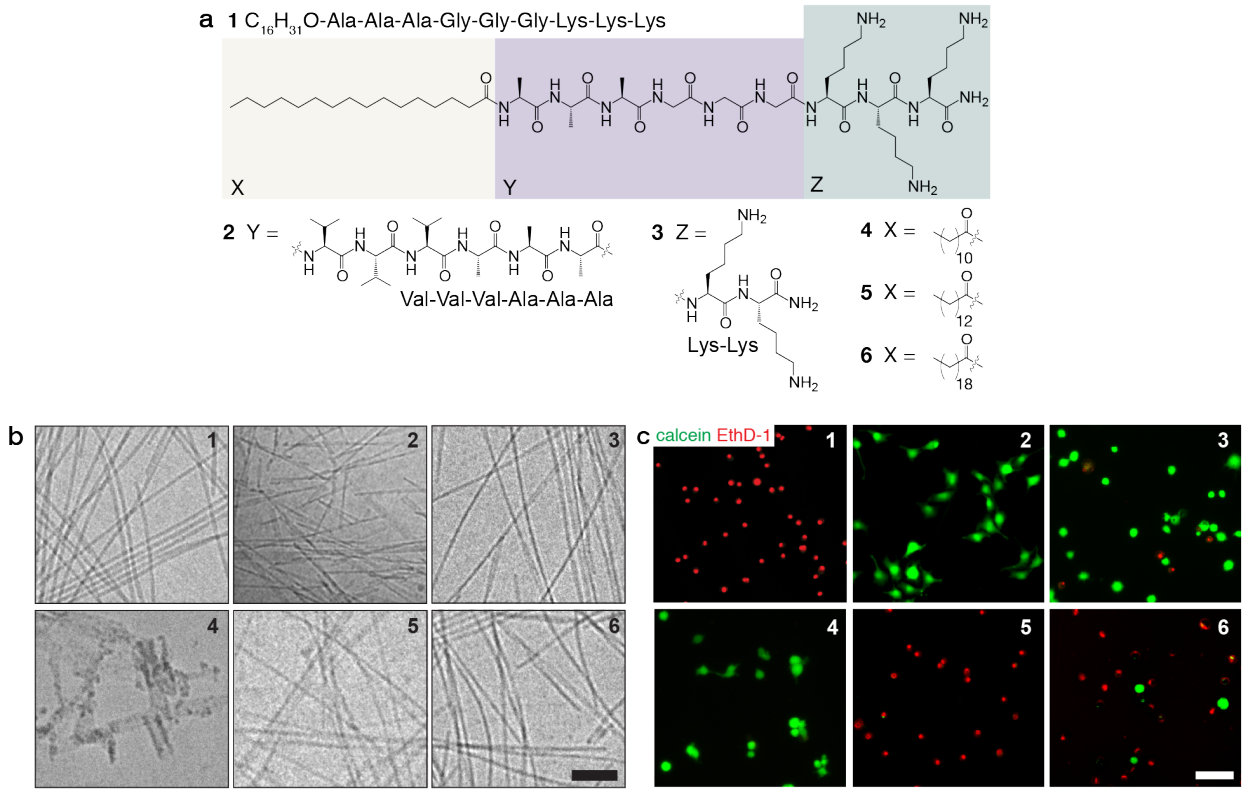

Supplementary Figure 1 | Molecular design of membrane-interacting self-assembling PA molecules. (**a**) Chemical structures of PAs that vary the β-sheet hydrogen bonding (PA **2**), the number of cationic lysine residues (PA **3**), and the alkyl tail length (PA **4** – PA **6**). (**b**) Representative cryogenic TEM images depicting the assembled morphology of each PA. Scalebar: 100 nm. (**c**) Representative fluorescence images of MC3T3-E1 cells that are viable (green, calcein AM) or dead (red, EthD-1) on coatings of each PA after 4 h of culture. Scalebar: 100 μm.

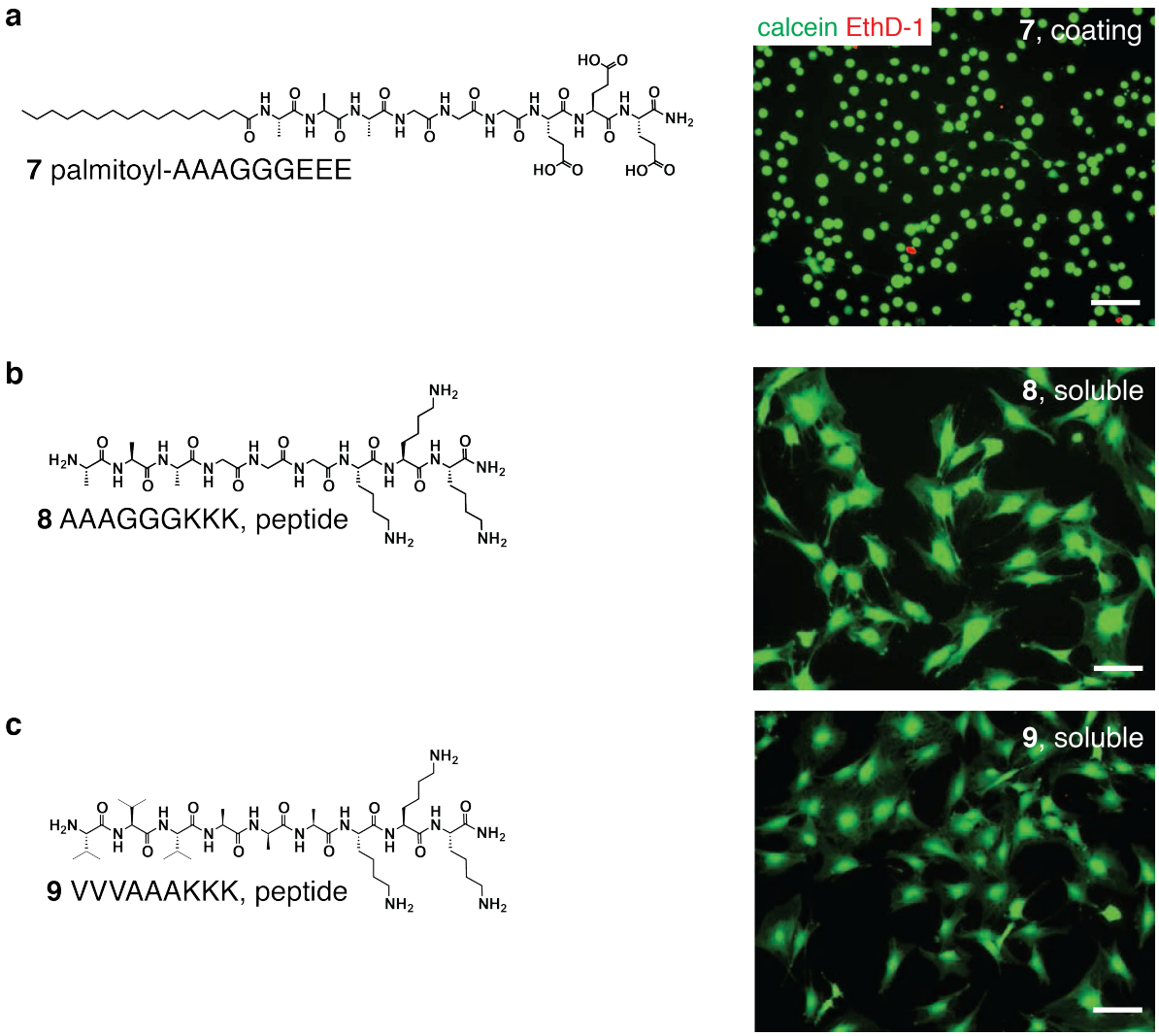

Supplementary Figure 2 | Cytotoxicity of a negatively charged analogue of PA 1 and the peptides corresponding to PA 1 and PA 2 without the alkyl tail. (**a**) Chemical structure of molecule **7**, an analogue of PA **1** where the lysine residues are replaced with glutamic acid (left) and the corresponding live-dead fluorescence image of MC3T3-E1 cells on a coating of PA **7** after 4 h of culture (right). (**b**) Chemical structure of molecule **8**, the peptide segment of PA **1** (left) and the corresponding live-dead fluorescence image of MC3T3-E1 cells with soluble peptide (0.05% wt) after 4 h of culture (right). (**c**) Chemical structure of molecule **9**, the peptide segment of PA **2** (left) and the corresponding live-dead fluorescence image of MC3T3-E1 cells with soluble peptide (0.05% wt) after 4 h of culture (right). All scalebars: 100 µm.

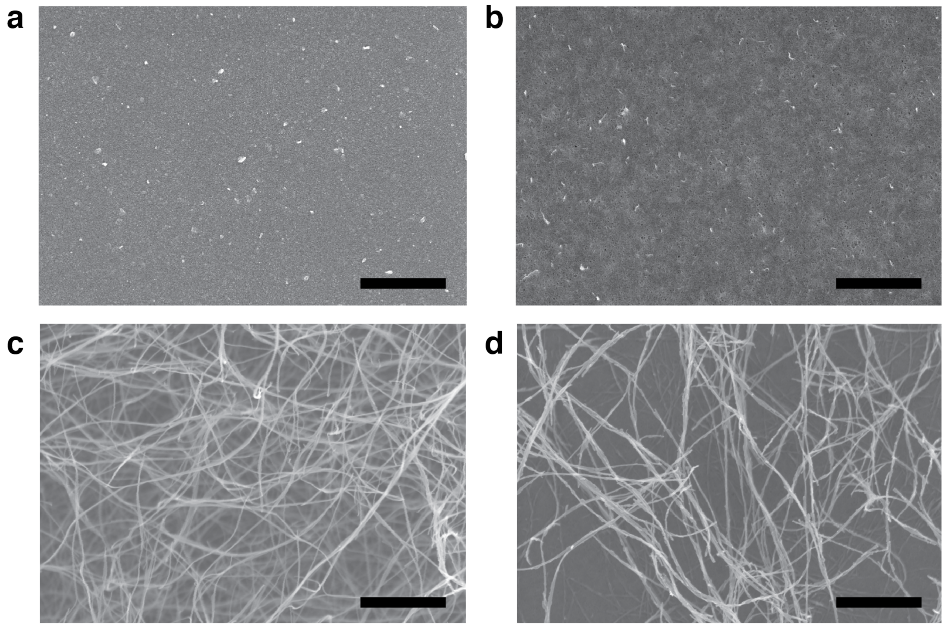

Supplementary Figure 3. Visualization of the PA coating process. Scanning electron microscopy of each step of the PA coating procedure. Glass coverslips are coated first with (a) poly-D-lysine followed by (b) sodium alginate, and then PA. Representative images of a (c) PA **1** coating and a (d) PA **2** coating show the presence of nanofibres. All scalebars: 2 μm.

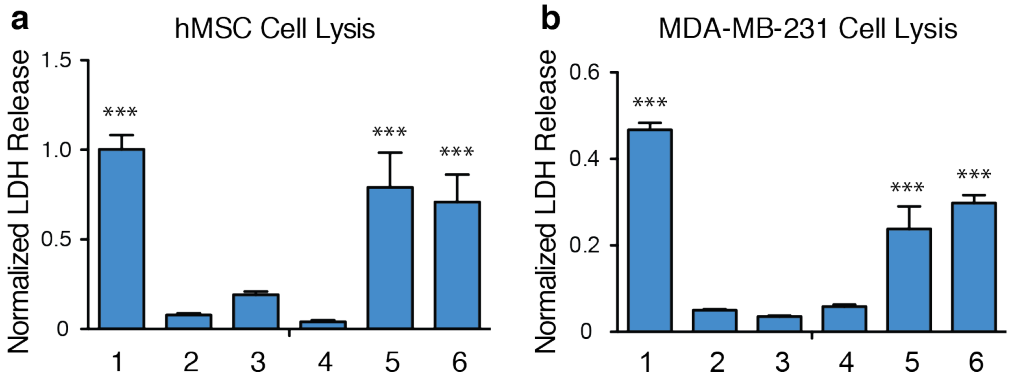

Supplementary Figure 4 | Cytotoxicity of PA coatings using different cell types. Cell viability was quantified by lactate dehydrogenase (LDH) release following 4 h in culture with (a) primary human mesenchymal stem cells (hMSC) or (b) the MDA-MB-231 breast cancer cell line. The trends in cell viability are similar to those observed with MC3T3-E1 cells. Chemical structures for PA **1** and PA **2** appear in the main text and chemical structures for PA **3**-**6** appear in Supplementary Figure 1. One-way ANOVA statistical analysis with Tukey post-test: comparison to PA **2** significance indicates release of lactate dehydrogenase, *** $p < 0.001$.

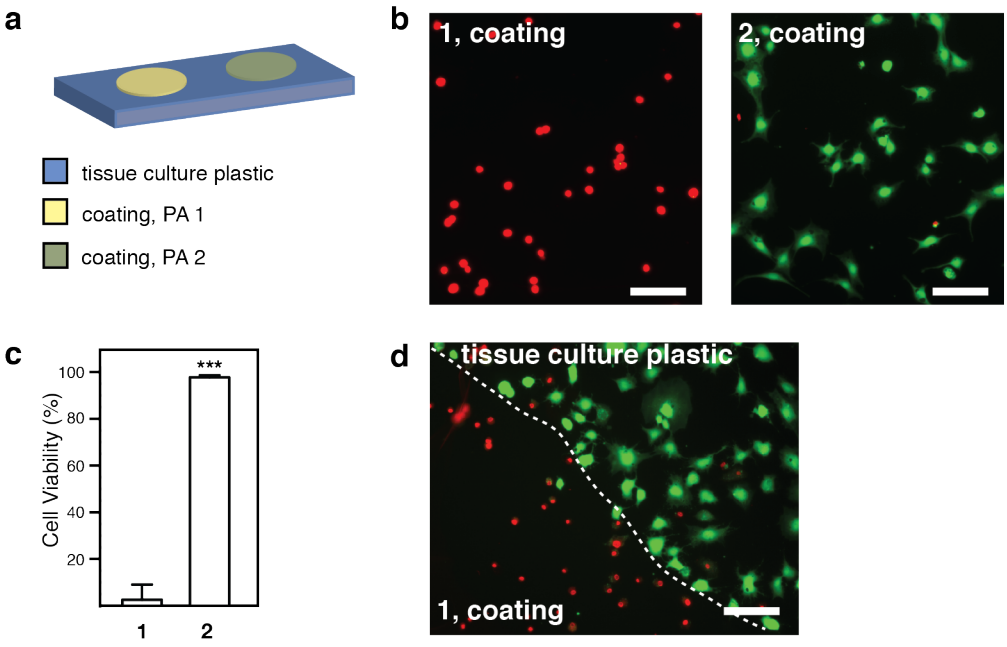

Supplementary Figure 5 | MC3T3-E1 cell viability when cultured on different PA coatings with shared culture medium. (**a**) Schematic of the experimental setup: Cells were seeded on PA **1**, PA **2** coatings on a single tissue culture dish. (**b**) Representative images stained with ethidium homodimer-1 (EthD-1, red) and calcein (green) showing that cells are viable on PA **2** coating, but dead on PA **1** coating, following 5 hours of culture. Scalebar: 100 µm. (**c**) Quantification of cell viability from experiments shown in (b) over three independent runs;statistical analysis: unpaired two tailed t-test, *** $p < 0.001$. (**d**) A representative calcein/EthD-1 stained image of the interface between the PA **1** coating and tissue culture plastic. Cells that are not in contact with the coating but located in close proximity remain viable after 5 hours of culture. The dotted white line represents the boundary between two surfaces. Scalebar: 200 µm.

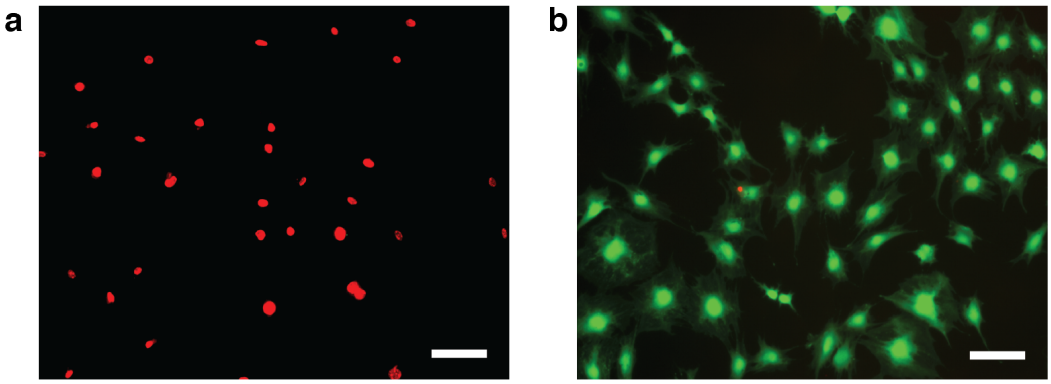

Supplementary Figure 6 | MC3T3-E1 cell viability when cultured with soluble PA. Representative fluorescence images after 4 h in culture showing cells seeded on tissue culture plastic and treated with 0.001%wt (a) PA **1** or (b) PA **2** in soluble form. Red: EthD-1, green: calcein AM. Scalebars: 100 µm.

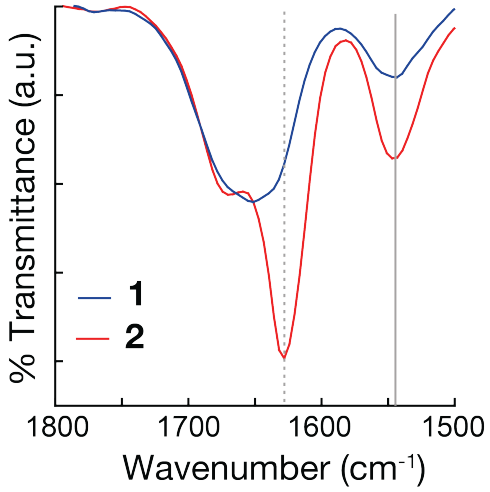

Supplementary Figure 7 | PA 2 exhibits β-sheet hydrogen bonding by attenuated total reflectance Fourier transform infrared spectroscopy. PA **2** exhibits stronger peaks at both of these amide I and amide II β-sheet stretches when compared with PA **1**. Dashed line: Amide I β-sheet stretch, solid line: Amide II β-sheet stretch.

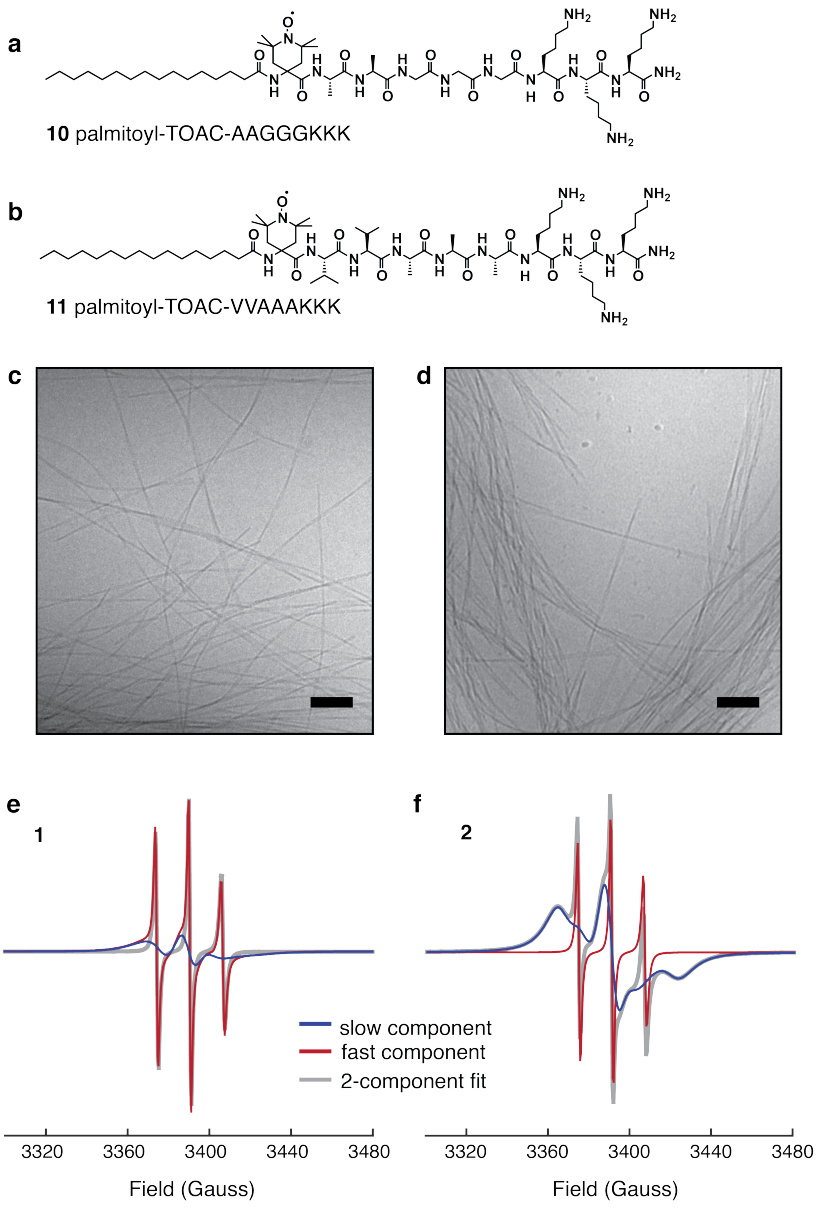

Supplementary Figure 8 | Details of electron paramagnetic resonance experiments. Chemical structures of the spin labeled analogues of (**a**) PA **1** with a weak β-sheet and (**b**) PA **2** with a strong β-sheet with a site specific spin label (TOAC) located at the first amino acid adjacent to the fatty acid tail to probe the β-sheet hydrogen bonding segment of the assemblies. (**c**.**d**)CryoTEM of 20% spin labeled PA combined with non-spin labeled PA used in EPR experiments. (**c**) PA **1** combined with its spin labeled analogue and (**d**) PA **2** combined with its spin labeled analogue. Scalebars: 100 µm. (**e**,**f**) Fits of electron paramagnetic resonance spectra from (**e**) PA **1** at a final concentration of 0.1%wt with molecule **10** and (**f**) PA **2** at a final concentration of 0.1%wt with molecule **11**. Data were fit using a non-linear least squares analysis (gray) and the slow (blue) and fast (red) components of the data are visualized.

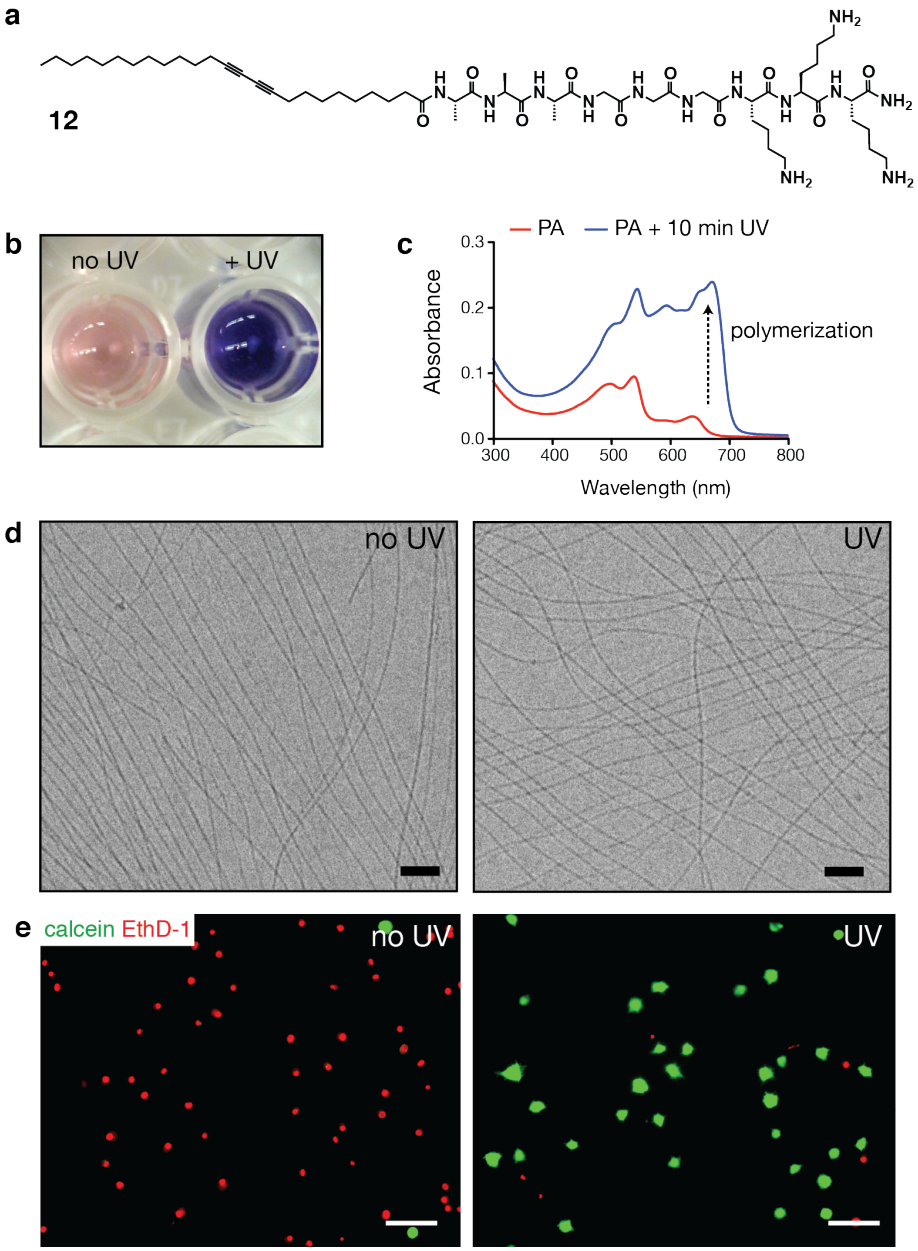

Supplementary Figure 9 | Design and characterisation of a UV-polymerizable analogue of the cytotoxic PA 1 to determine if cohesion could be implemented through crosslinking the PA lipid core. (**a**) Chemical structure of the UV-polymerizable PA that has a diacetylene group in the lipid tail. (**b**) Color change upon UV exposure shows a clear difference in absorbance indicating crosslinking between diacetylene units. (**c**) UV-vis demonstrating increased intensity of the polymerized peak upon exposure to UF for 10 minutes. (**d**) Cryogenic TEM shows that the molecule assembles into nanofibres both (left) prior to UV treatment and (right) following UV treatment at 0.1% (w/v) in water. Scalebars: 100 nm. (**e**) Representative fluorescent images of MC3T3-E1 cells that are live (green, calcein) or dead (red, EthD-1) cultured on coatings of the UV-polymerizable PA for 4 h. Without UV treatment (left), the PA coatings are toxic while UV-treated coatings (right) supported cell viability. Scalebars: 100 µm.

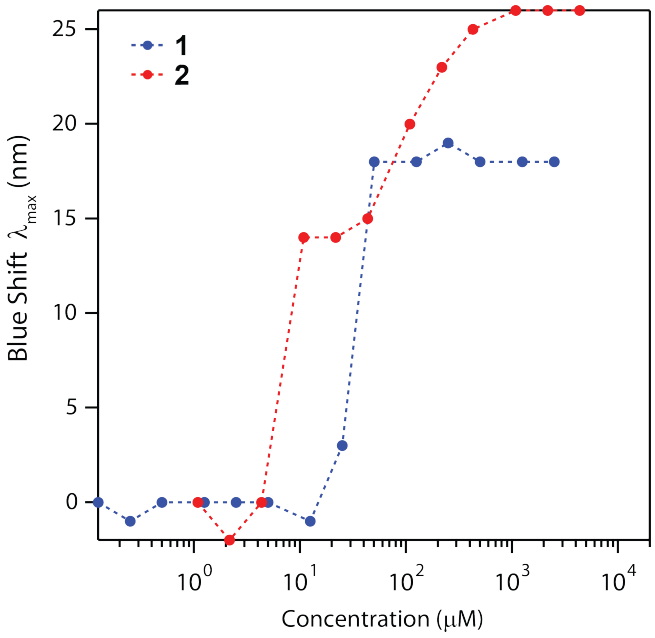

Supplementary Figure 10 | Aggregation behavior as a function of concentration of PA 1 and PA 2 determined using the Nile Red assay. Both PA **1** and PA **2** demonstrate similar profiles for aggregation. The critical aggregation concentrations are on the same order of magnitude.

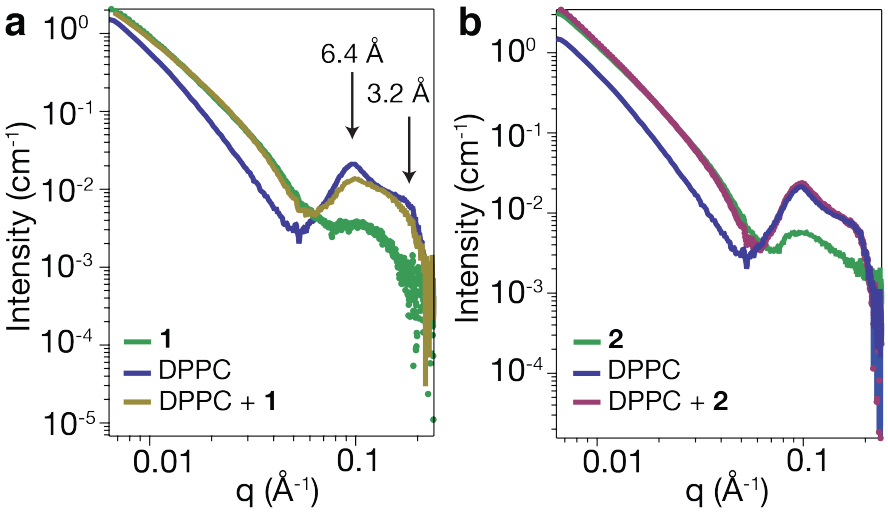

Supplementary Figure 11 | Small angle X-ray scattering PA- DPPC liposome mixtures to evaluate differences in liposome lamellarity. SAXS scattering profiles in absolute units of (**a**) multilamellar DPPC liposomes combined with PA **1** and (**b**) multilamellar DPPC liposomes combined with PA **2**. The Bragg peaks at 6.4 Å and 3.2 Å represent periodic spacing between lamellae. Upon addition of PA **1**, these peaks diminish while no differences in the peak height or shape are present upon addition of PA **2**.

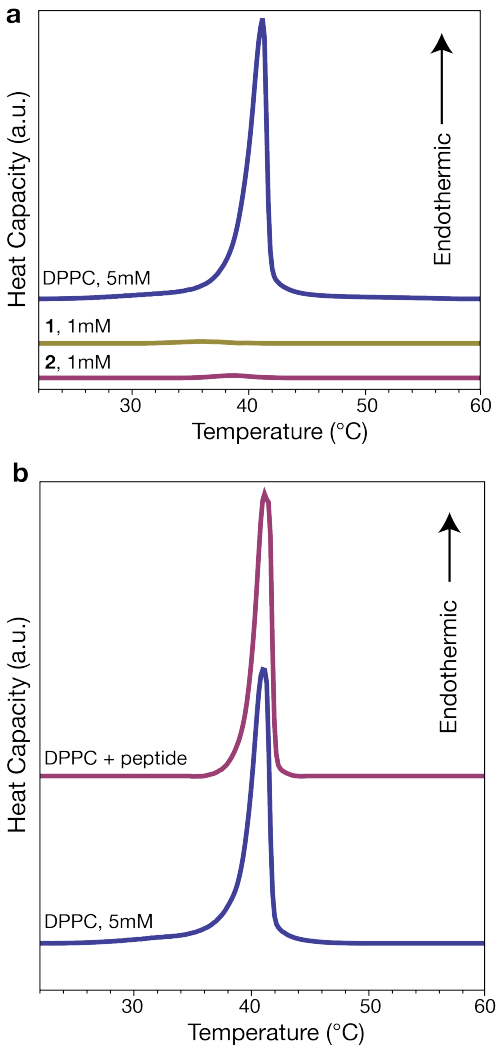

Supplementary Figure 12 | Differential scanning calorimetry of controls including PA and lipid combined with the non-toxic peptide. (**a**) DSC thermograms of PA **1** and PA **2** at 1 mM, the concentration used with liposome-PA mixtures demonstrating minimal signal compared to lipid alone (DPPC). (**b**) DSC thermograms of DPPC liposomes mixed with the control molecule (molecule **8**) containing the peptide segment of PA **1**. The lipid melting temperature and the intensity of the peak corresponding to the main phase transition of DPPC is unperturbed demonstrating the importance of the alkyl tail for interaction with lipid.

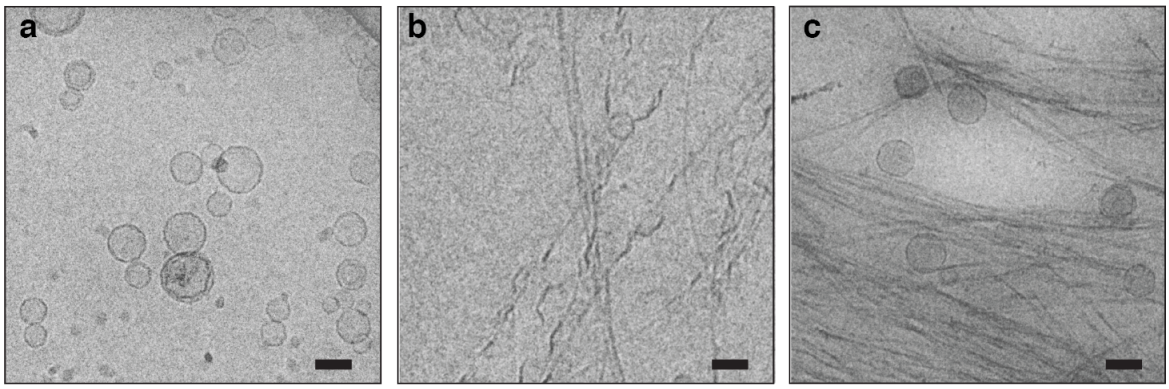

Supplementary Figure 13 | Morphology of liposome PA mixtures following differential scanning calorimetry measurements. Cryogenic transmission electron micrographs of (**a**) DPPC liposomes alone, (**b**) DPPC liposomes with PA **1**, and (**c**) DPPC liposomes with PA **2** following DSC. These images show similar trends in morphology prior to heating and cooling cycles (heated to 60 °C and cooled to 25 °C). The DPPC liposomes alone remain intact following temperature cycling and demonstrate disrupted morphologies in the presence of PA **1**. In the presence of PA **2**, both intact liposomes and fibers are present. Scalebars: 100 nm.

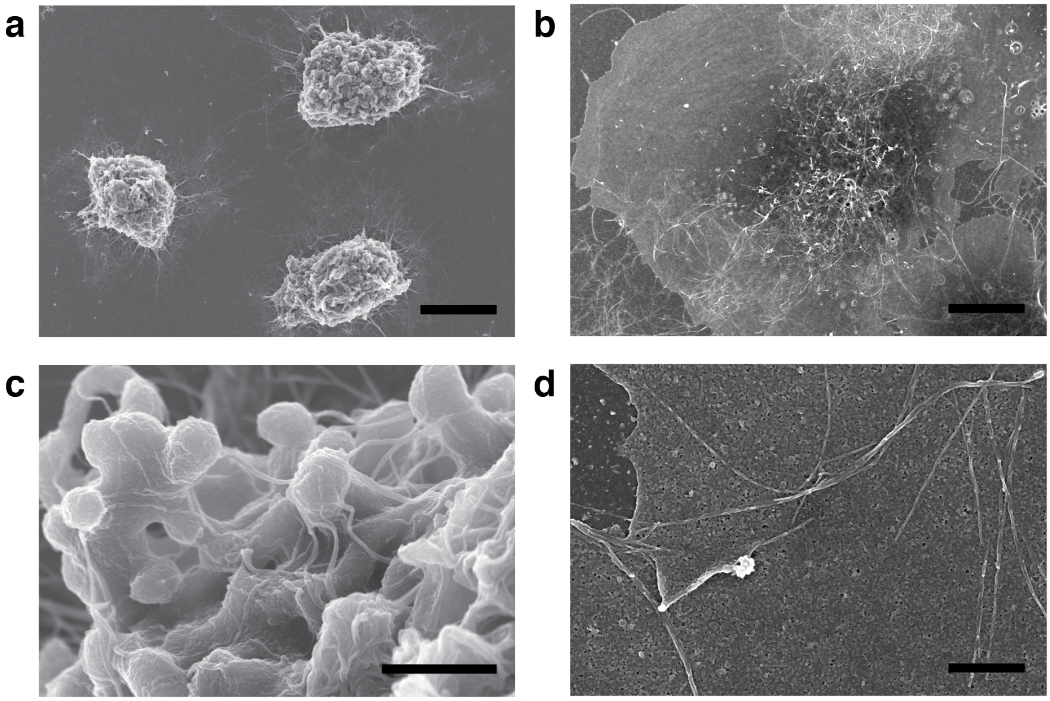

Supplementary Figure 14 | Scanning electron microscopy images of MC3T3-E1 cells seeded on poly-D-lysine coated glass coverslips and exposed to 0.01% (w/v) soluble PA for 30 minutes. (**a,b**) Low magnification images with PA **1** or PA **2** Scalebars: 10 µm. (**c,d**) Higher magnification images showing the presence of PA nanofibres on the cell surface with both PA **1** and PA **2**, respectively**.**
Scalebars: 1 µm.

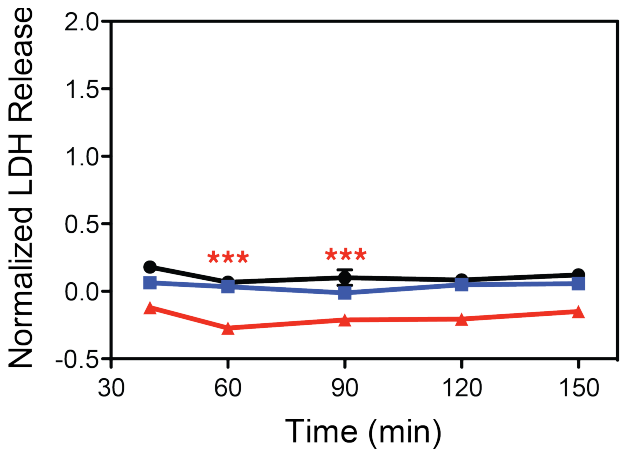

Supplementary Figure 15 | LDH release profiles from MC3T3-E1 cells on coatings of PA 2. Cells do not exhibit a trend of increased LDH release over the first 150 minutes of culture on PA **2** coatings. Cells remain intact and do not release LDH following actin inhibition (blue) or myosin inhibition (red) when compared to untreated controls (black). One-way ANOVA with Dunnett post test ***$p < 0.001$ Colored asterisks correspond to the same colored condition with significance compared to untreated control.

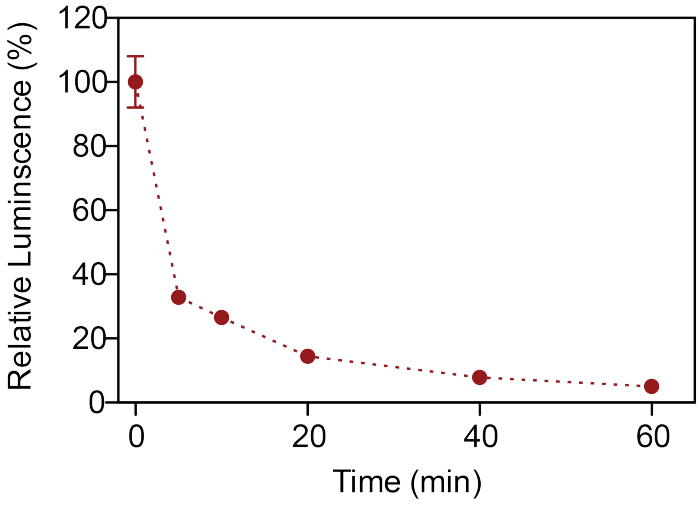

Supplementary Figure 16 | Determination of ATP depletion using MC3T3-E1 cells. Results from an ATP luminescence assay demonstrate that cells treated for ATP depletion exhibit ATP levels of approximately 5% of untreated cells after 1 h of treatment. Cells were added to coatings after 1 h of treatment.

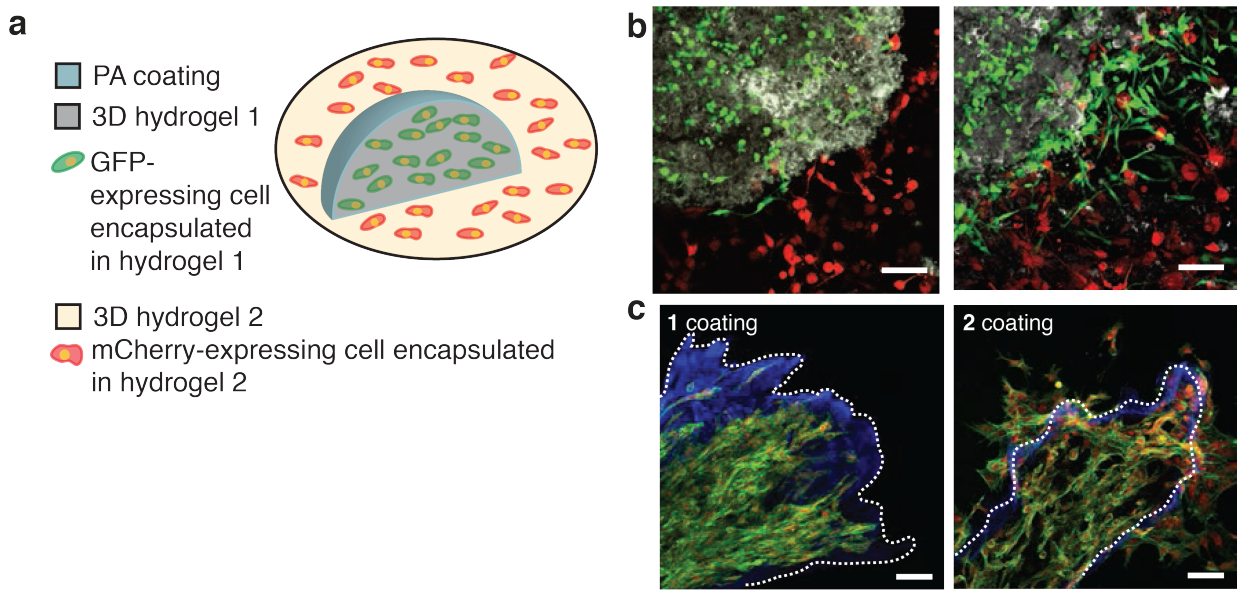

Supplementary Figure 17 | Implementation of PA coatings with varying β-sheet to serve as a cell barrier with MB-MDA-231 cells. (**a**) Experimental setup where GFP expressing MB-MDA-231 breast cancer cells are encapsulated in a negatively charged hydrogel 1 (Anionic PA, palmitoyl-VVAAEE) then coated with either PA **1** or PA **2**. This material is then and placed in a second hydrogel 2 (collagen) encapsulated with mCherry expressing MB-MDA-231 breast cancer cells to evaluate if cells escape from the gels and cause mixing of cell types. (**b**) A maximum intensity projection of a confocal stack of the setup in (**a**) showing the both GFP and mCherry cells are present in the collagen matrix after 3 days in culture. (**c**) Using a similar setup with acellular collagen and MC3T3-E1 cells encapsulated in hydrogel 1 after 7 days in culture. Staining for actin (phalloidin, green) and nuclei (propidium iodide, red) demonstrate that cells are retained in hydrogel 1 (blue) coated with the toxic PA **1** while cells escape into the surrounding collagen in gels coated with PA **2**. The white dashed line indicates the boundary between the PA gel and the collagen gel. All scalebars: 100 µm.

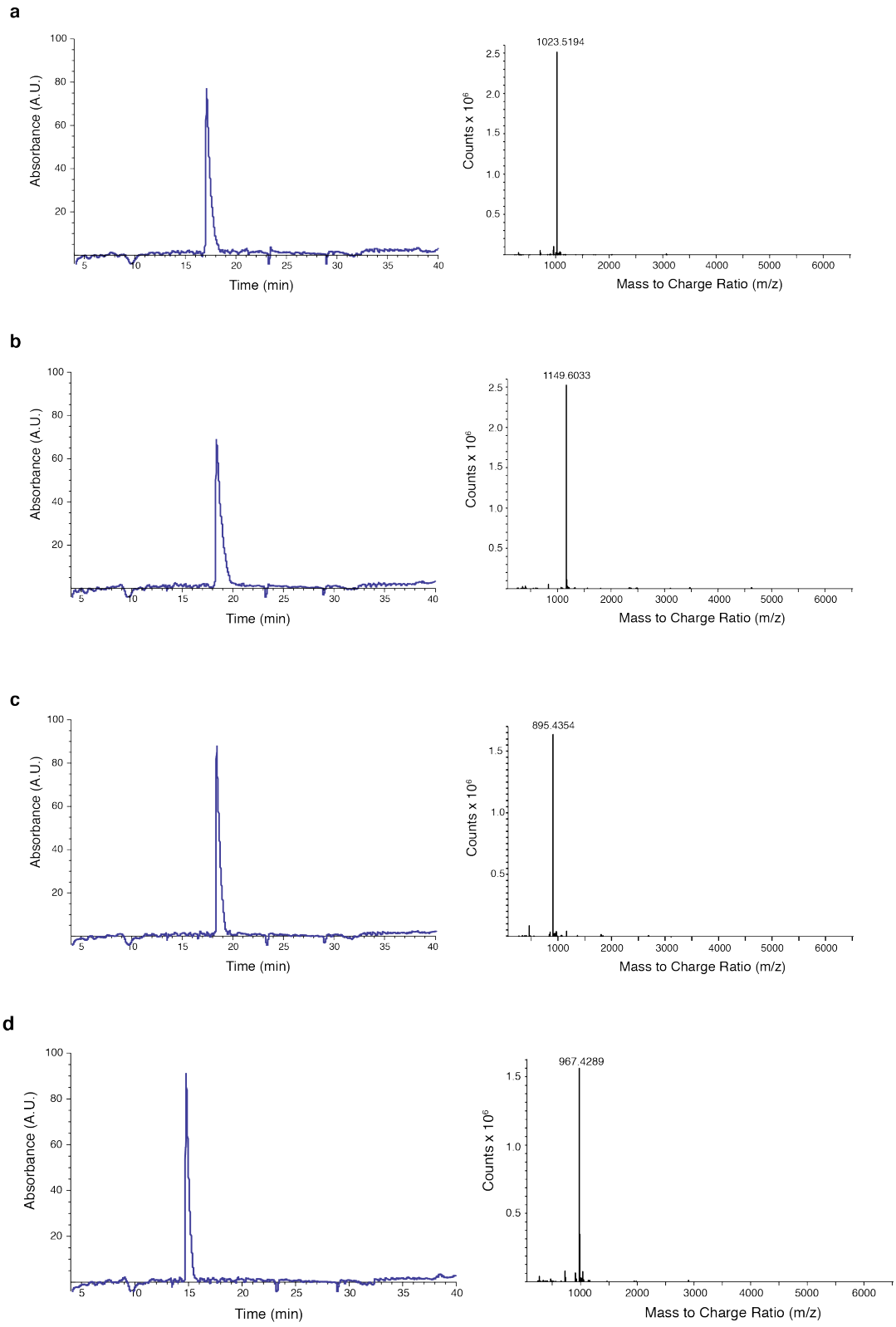
a
Absorbance (A.U.)
Time (min)
1023.5194
Counts x 10^6
Mass to Charge Ratio (m/z)
b
Absorbance (A.U.)
Time (min)
1149.6033
Counts x 10^6
Mass to Charge Ratio (m/z)
c
Absorbance (A.U.)
Time (min)
895.4354
Counts x 10^6
Mass to Charge Ratio (m/z)
d
Absorbance (A.U.)
Time (min)
967.4289
Counts x 10^6
Mass to Charge Ratio (m/z)

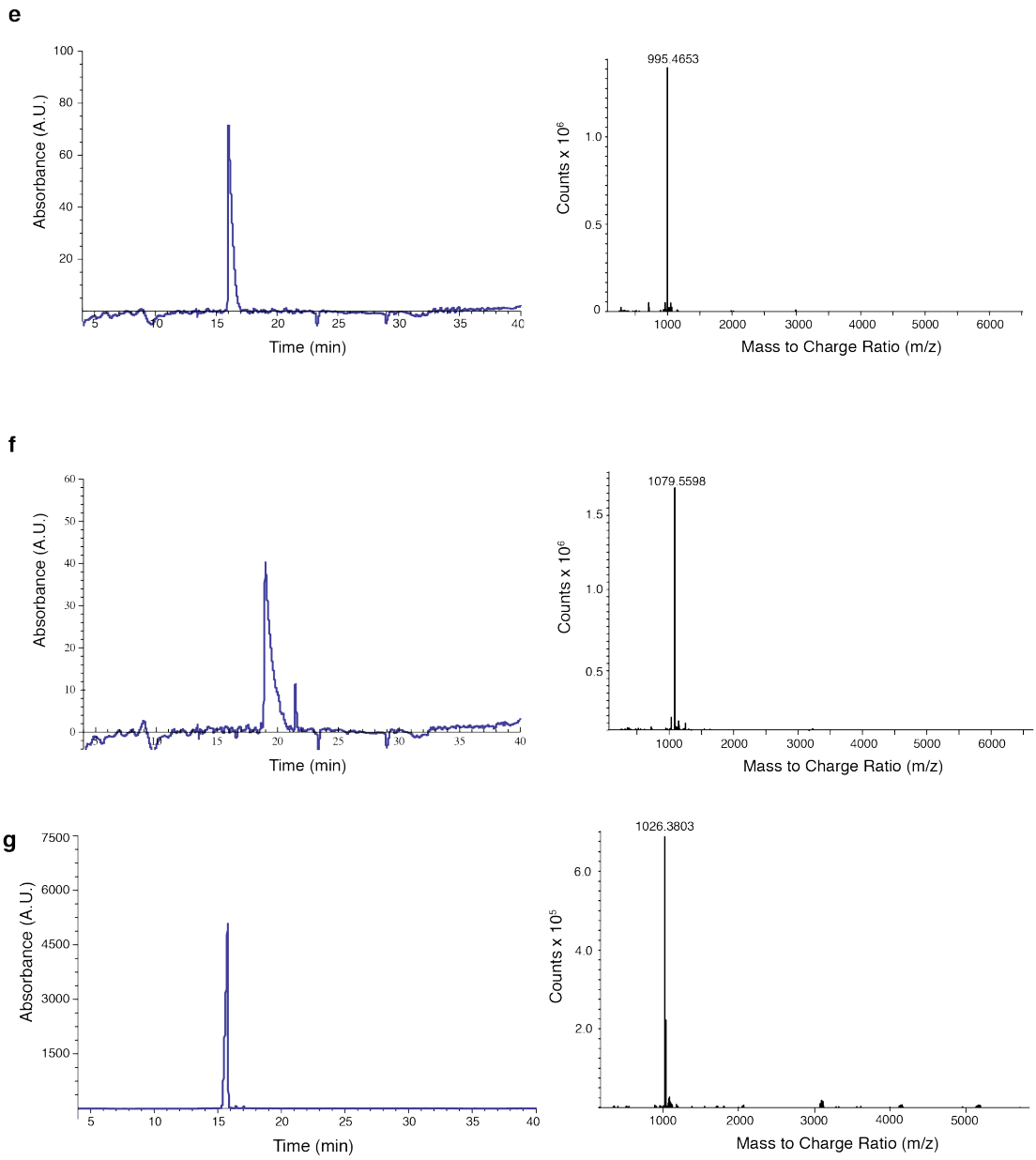

Supplementary Figure 18 | Mass determination and characterisation of molecular variations of PA 1. High performance liquid chromatography traces (left) and mass spectrometry (right) of (**a**) PA **1**, MS (*m/z*) $[M]^+$ calc'd. for $C_{45}H_{85}N_{13}O_{10}$, 1023.72; found, 1023.52, (**b**) PA **2**, MS (*m/z*) $[M]^+$ calc'd. for $C_{47}H_{89}N_{13}O_{10}$, 1149.86; found, 1149.60, (**c**) PA **3**, MS (*m/z*) $[M]^+$ calc'd. for $C_{43}H_{81}N_{11}O_9$, 895.62; found, 895.44, (**d**) PA **4**, MS (*m/z*) $[M]^+$ calc'd. for $C_{45}H_{85}N_{13}O_{10}$, 967.65; found, 967.43, (**e**) PA **5**, MS (*m/z*) $[M]^+$ calc'd. for $C_{47}H_{89}N_{13}O_{10}$, 995.69; found, 995.47, (**f**) PA **6**, MS (*m/z*) $[M]^+$ calc'd. for $C_{53}H_{101}N_{13}O_{10}$, 1079.78; found, 1079.56, (**g**) PA **7**, MS (*m/z*) $[M]^+$ calc'd. for $C_{46}H_{78}N_{10}O_{16}$, 1026.56; found, 1026.38.

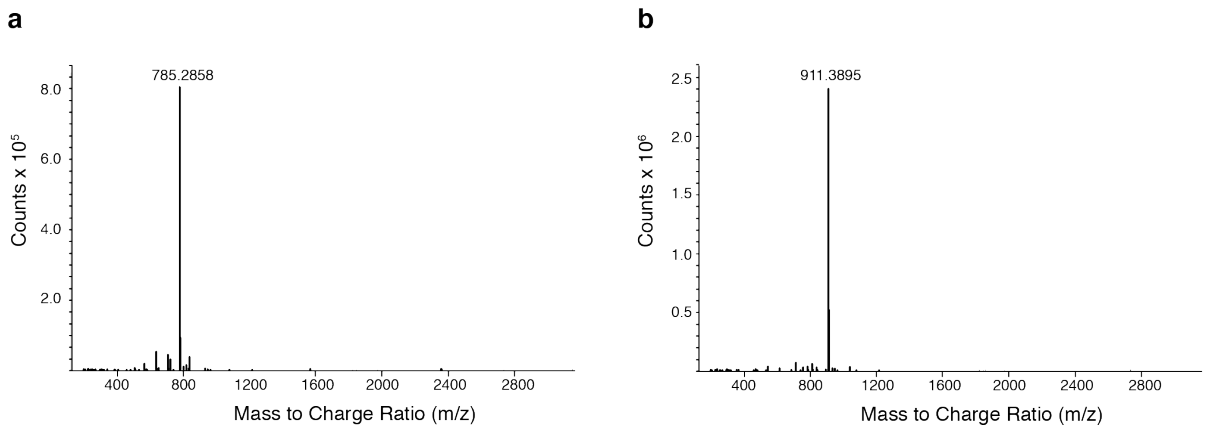

Supplementary Figure 19 | Mass determination and characterisation of peptide analogues of PA 1 and PA 2. Mass spectrometry of (**a**) molecule **8**, the peptide analogue of PA **1**, MS (*m/z*) $[M]^+$ calc'd. for $C_{33}H_{63}N_{13}O_9$, 785.49; found, 785.23, and (**b**) molecule **9**, the peptide analogue of PA **2**, MS (*m/z*) $[M]^+$ calc'd. for $C_{42}H_{81}N_{13}O_{10}$, 911.63; found, 911.39.

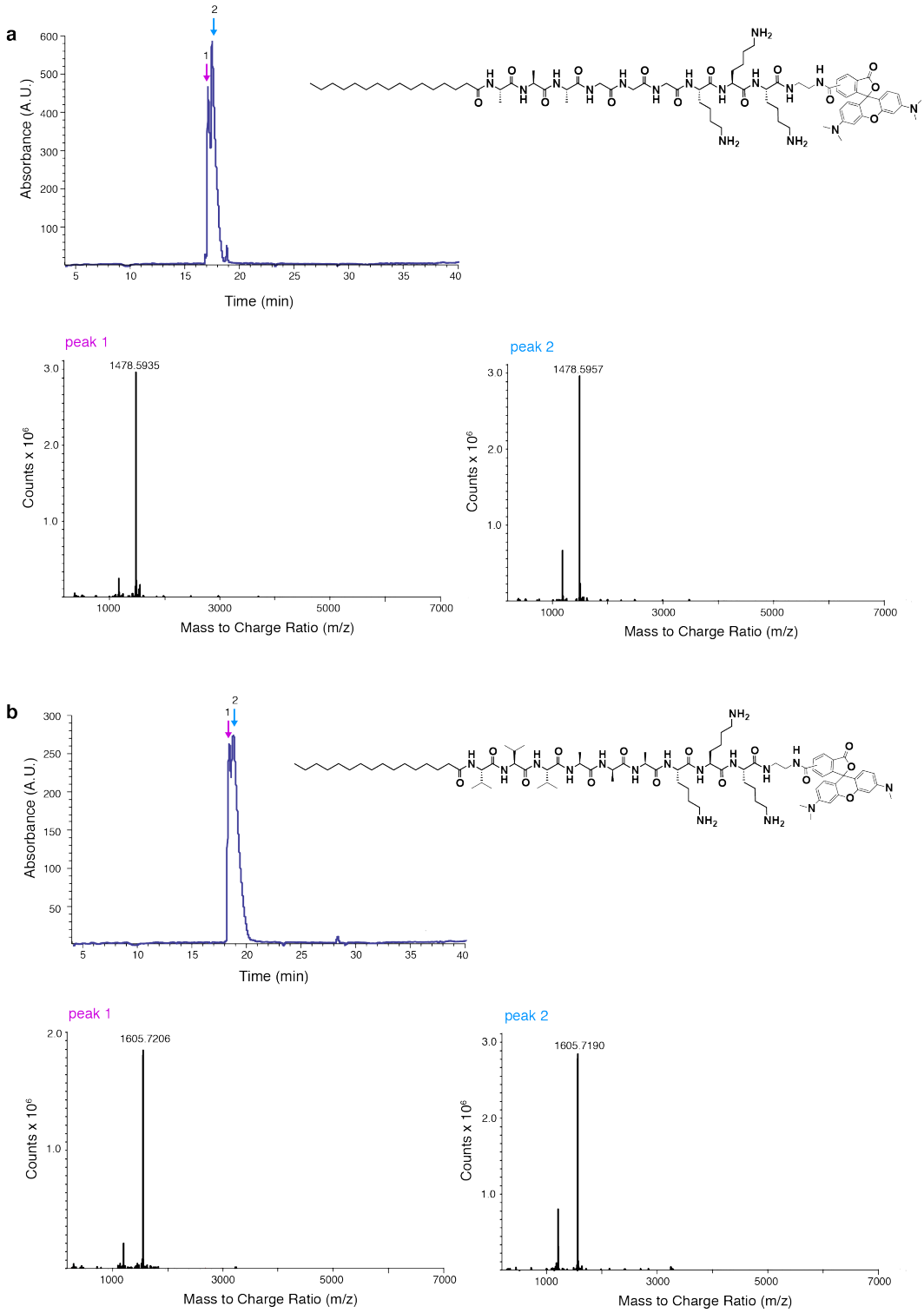

Supplementary Figure 20 | Mass determination and characterisation of fluorescent analogues of PA 1 and PA 2. Mass spectrometry of (**a**) the fluorescent analogue of PA **1**, MS (*m/z*) $[M]^+$ calc'd. for $C_{78}H_{118}N_{16}O_{14}$, 1478.9; found, 1478.59, 1478.60, and (**b**) the fluorescent analogue of PA **2**, MS (*m/z*) $[M]^+$ calc'd. for $C_{85}H_{136}N_{16}O_{14}$, 1605.04; found, 1605.72, 1605.72. Two isomers of the same molecule were identified.

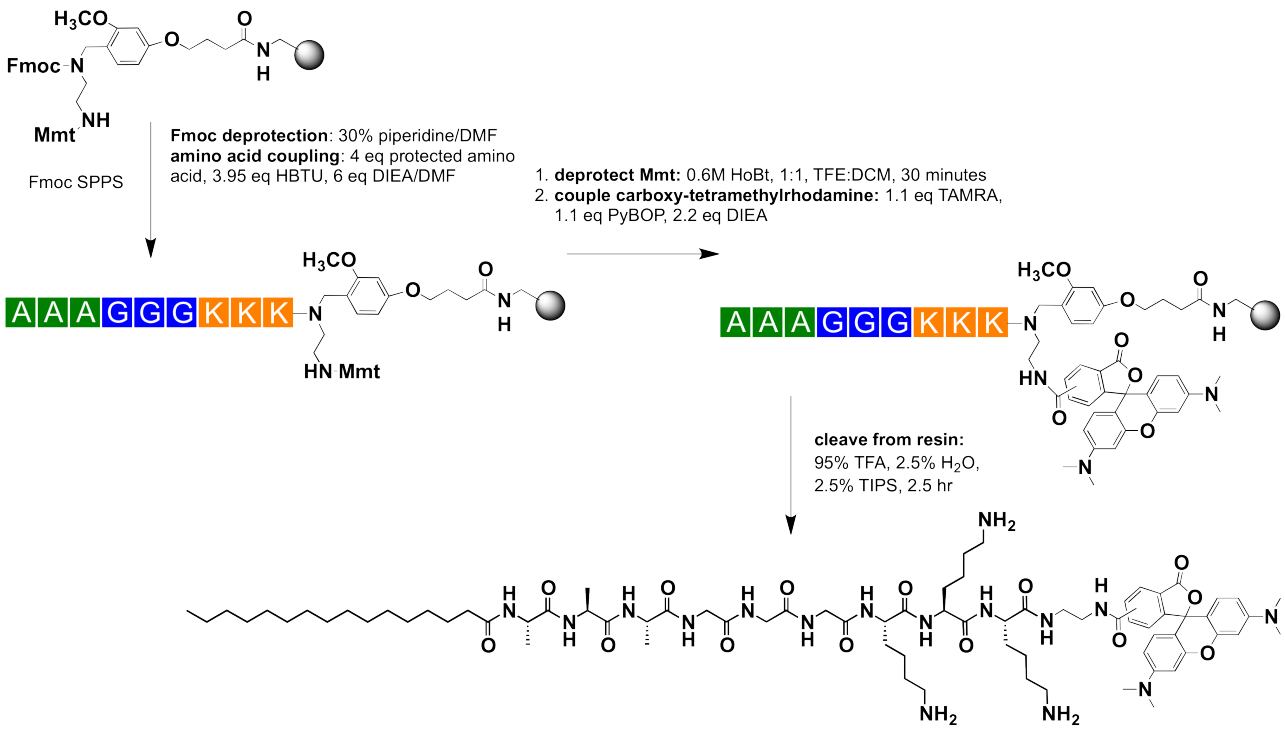

Supplementary Figure 21 | Schematic of the method used to synthesize fluorescently labeled PA 1. Step by step synthesis to synthesize fluorescently labeled PA. The same method was used to synthesize the fluorescent PA **2**. A: SPPS: solid-phase peptide synthesis, Mmt:monomethyoxytrityl, DMF: dimethylformamide, HBTU: O-(benzotriazol-1-yl)-N,N,N',N'-tetramethyluronium hexafluorophosphate, DIEA: N,N-diisopropylethylamine, TFE: trifluoroethanol, DCM: dichloromethane, TAMRA: 5(6)-carboxy-tetramethylrhodamine, PyBOP: benzotriazol-1-yl-oxytripyrrolidinophosphonium hexafluorophosphate, TFA: trifluoroacetic acid, TIPS: triisopropylsilane.

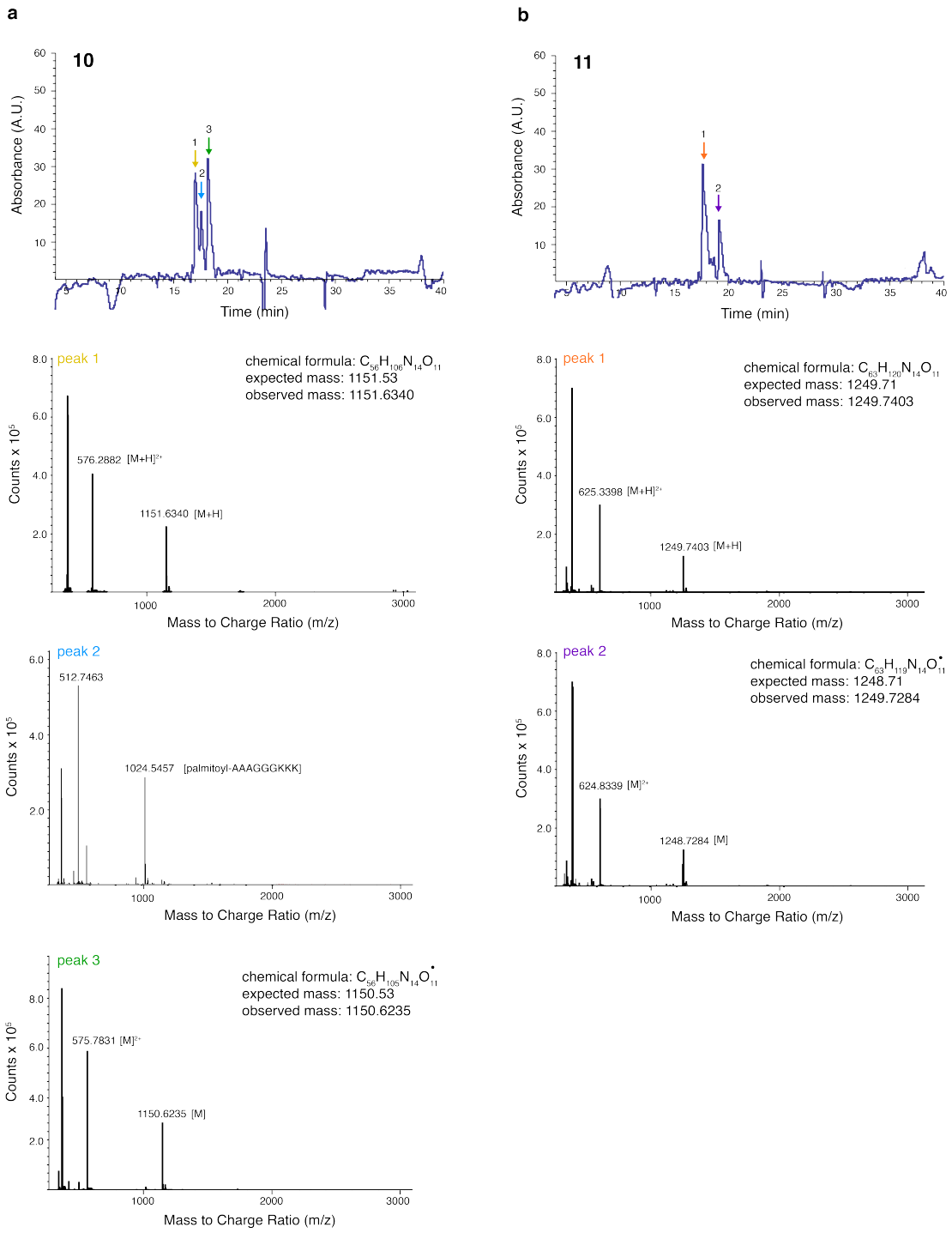

Supplementary Figure 22 | Mass determination and characterisation of spin labeled analogues of PA 1 and PA 2. High performance liquid chromatography and mass spectrometry of (**a**) PA **10**, the spin labeled analogue of PA **1**, MS (*m/z*) $[M]^+$ calc'd. for $C_{56}H_{106}N_{14}O_{11}^{\bullet}$, 1151.53; found, 1151.63, 1024.55, $[M]^+$ calc'd. for $C_{56}H_{106}N_{14}O_{11}$, 1150.53; found, 1150.62, and (**b**) PA **11**, the spin labeled analogue of PA **2**, MS (*m/z*) $[M]^+$ calc'd. for $C_{63}H_{119}N_{14}O_{11}^{\bullet}$, 1249.71; found, 1249.74, MS (*m/z*) $[M]^+$ calc'd. for $C_{63}H_{119}N_{14}O_{11}$, 1248.71; found, 1248.73. The acidic conditions of HPLC cause reduction of the free radical.

Supplementary Methods

Attenuated total reflectance-Fourier transform infrared spectroscopy. ATR-FTIR was performed using a Bruker Tensor 37 spectrometer fitted with a germanium crystal pike cell accessory. PA was dissolved in water at 1% (w/v) and were deposited on the germanium crystal and measured. Solvent background was subtracted from the final data.

Small-angle X-ray Scattering. Small-angle X-ray Scattering (SAXS) measurements were performed at the Advanced Photon Source at Argonne National Laboratory using an insertion device beamline 5-ID-D Dupont-Northwestern-Dow Collaborative Access team. To compare the scattering from PA with mixtures of DPPC and PA, samples were injected through a capillary tube flow cell at room temperature to maintain a constant sample volume and sample to detector distance. Data were collected at an incident photon energy of 15kV using an exposure time of 10 seconds. The sample was flowing during data collection to reduce radiation damage and 5 total scans were acquired and averaged. The scattering intensity was recorded with a q range of $0.008 < q < 0.25$ Å^{-1} where the wave vector q was defined as $q = (4\pi/\lambda)\sin(\theta/2)$ where θ is the scattering angle. Two-dimensional SAXS data was radially averaged to produce one-dimensional intensity profiles using FIT2D. Conversion to absolute units was enabled by also measuring the scattering from an empty capillary and capillary filled with solvent.

To evaluate the morphology of the PA assemblies, quartz capillaries (Charles Supper, 1.5 mm outer diameter, 0.01 mm wall thickness) were filled with solutions of PA at 0.5% (w/v) in a 1:1 mixture of water:MEM-Alpha media. Using a 15kV energy, data was collected using an exposure time of 6-10 seconds. The scattering intensity was recorded with a q range of $0.008 < q < 0.25$ Å^{-1} where the wave vector q was defined as $q = (4\pi/\lambda)\sin(\theta/2)$ where θ is the scattering angle. Two-dimensional SAXS data was radially averaged to produce one-dimensional intensity profiles using FIT2D. For background subtraction, scattering profiles were obtained for capillaries filled with solvent. No attempt was made to convert the units to an absolute scale. Data interpretation was performed using the NCNR Irena package.